A VERTICALLY AVERAGED SPECTRAL MODEL FOR TIDAL CIRCULATION IN ESTUARIES: PART 1. MODEL FORMULATION

By Jon R. Burau and Ralph T. Cheng

U.S. GEOLOGICAL SURVEY

Water-Resources Investigations Report 88-4126

Prepared in cooperation with the
CALIFORNIA STATE WATER RESOURCES CONTROL BOARD and the
CALIFORNIA DEPARTMENT OF WATER RESOURCES

3024-02

Sacramento, California
1989

DEPARTMENT OF THE INTERIOR

MANUEL LUJAN, JR., Secretary

U.S. GEOLOGICAL SURVEY

Dallas L. Peck, Director

For additional information
write to:

District Chief
U.S. Geological Survey
Federal Building, Room W-2234
Sacramento, CA 95825

Copies of this report can
be purchased from:

U.S. Geological Survey
Books and Open-File Reports Section
Federal Center, Building 810
Box 25425
Denver, CO 80225

CONTENTS

ILLUSTRATIONS

COVER: A computer-generated graph illustrates the shape of the bottom of San Francisco Bay. Vertical scale is exaggerated a factor of 800.

CONVERSION FACTORS

The metric (International System) units are used in this report. For those readers who prefer to use the inch-pound system, the conversion factors for the terms used in this report are listed below:

Multiply metric unit	By	To obtain inch-pound unit
meter (m)	3.281	feet (ft)
kilometer (km)	0.6214	mile (mi)
meters per second (m/s)	3.281	feet per second (ft/s)

Sea level: In this report "sea level" refers to the National Geodetic Vertical Datum of 1929 (NGVD of 1929)--a geodetic datum derived from a general adjustment of the first-order level nets of both the United States and Canada, formerly called Sea Level Datum of 1929.

A VERTICALLY AVERAGED SPECTRAL MODEL FOR TIDAL CIRCULATION IN ESTUARIES: PART 1. MODEL FORMULATION

By Jon R. Burau and Ralph T. Cheng

ABSTRACT

A frequency dependent computer model based on the two-dimensional vertically averaged shallow-water equations is described for general application in tidally dominated embayments. This model simulates the response of both the tides and tidal currents to user-specified geometries and boundary conditions. The mathematical formulation and practical application of the model are discussed in detail. Salient features of the model include the ability to specify (1) stage at the open boundaries as well as within the model grid, (2) velocities on open boundaries (river inflows and so forth), (3) spatially variable wind stress, and (4) spatially variable bottom friction. Using harmonically analyzed field data as boundary conditions, this model can be used to make real time predictions of tides and tidal currents.

INTRODUCTION

This report describes the theoretical background and formulation of a computer program that solves the linearized shallow-water equations using a spectral approach. In this model the shallow-water equations are modified into a time-independent form after assuming that the tides and tidal currents are harmonic functions in time. This model was developed for hydrodynamic studies of San Francisco Bay, California, as part of an inter-agency modeling effort supported in part by the California State Water Resources Control Board and the California Department of Water Resources. Historically, circulation modeling in San Francisco Bay has been done separately on individual subembayments within the overall system (Cheng and Casulli, 1982; and Smith and Cheng, 1987). Application of traditional time-stepping methods to solve the nonlinear shallow-water equations at the spatial resolution necessary to represent the bathymetry of San Francisco Bay is beyond the practical limit of available computer resources, particularly when simulations of many tidal cycles are considered. However, San Francisco Bay as an overall system is considered a weakly nonlinear system; therefore, much of its response to tidal forcing is nearly linear. By neglecting nonlinear terms in the governing shallow-water equations, the spectral model equations become linear. These linear equations then can be efficiently solved in the frequency domain without resorting to time-stepping procedures. When the spectral model equations are approximated using the finite-element method, a very detailed spatial distribution of the flow properties can be obtained by using a sufficiently fine computational grid. As an alternative to solving the full system of equations for the entire San Francisco Bay system, a frequency based algorithm, a spectral model, was developed.

Literature Review and Model Overview

Time-stepping models have been used for years to solve many practical coastal and estuarine circulation problems. Typically, the primitive and nonconservative forms of the depth-averaged shallow-water equations have been solved using either finite-difference methods (Leendertse and Gritton, 1971) or hybrid methods which employ finite-element techniques in space and finite-difference methods in time (King and others, 1973; Gray and Lynch, 1977; and Cheng, 1978). Over the past few years, solutions of the full three-dimensional shallow-water equations have been attempted (Blumberg and Mellor, 1981; and Sheng, 1983). Use of these models still is not practical because of huge data requirements and the computer time needed to run three-dimensional models.

The shallow-water equations can be rearranged into the form of a wave equation (Lynch and Gray, 1979) by substituting the conservative form of the momentum equations into the time derivative of the continuity equation. The principal advantage of a wave-equation model is that numerical noise or spurious oscillations, often found in discrete solutions to the shallow-water equations when applied to complex geometries, are reduced (Platzman, 1981; Gray and Lynch, 1979; and Cunge and others, 1980).

Models based on the wave equation and models that solve the primitive or nonconservative shallow-water equations require repeated solution with time, making them computationally inefficient. For these time-stepping models, the time step is generally limited by either a stability condition or an accuracy requirement that determines the maximum allowable time step (Roache, 1982). Therefore, application of time-stepping methods to problems involving long-term simulations (on the order of several days) with detailed numerical grids can be computationally impractical, if not impossible. To resolve this dilemma, spectral models, which circumvent the need to step with time, are increasingly being used in estuarine studies.

Spectrum, or spectral, models were first outlined by Hansen (1950), although earlier work on this general formulation is variously credited to Defant (1919). Hansen (1950) describes a formulation based on the assumption that the total tidal energy at any given point can be represented by the summation of partial tides. This basic approach has been applied for years by the National Oceanic and Atmospheric Administration (Schureman, 1985; and Dennis and Long, 1971), the U.S. Geological Survey (Cheng and Gartner, 1985), and others who harmonically decompose tides and tidal currents into partial tides of known frequency.

Pearson and Winter (1977) and Westerlink and others (1983) rearranged the shallow-water equations into a linear group and a nonlinear group. They assume that the time-dependent variables in the linear group are periodic and can be represented by frequency-dependent Fourier components. The linear terms then are solved in the frequency domain (a spectral approach) while the nonlinear terms are solved iteratively at each step in time. Their method uses Fourier techniques to obtain the solutions, wherein the solutions are subsequently analyzed to determine the dominant frequencies. The strength of this approach is in the inclusion of the nonlinear terms. Unfortunately, this is achieved at the expense of a time-dependent solution requiring iteration at each time step.

Le Provost and Poncet (1978) present a spectral method based on a perturbation technique in which the quadratic friction term is represented using a generalized Fourier series involving elliptic integrals. Snyder and others (1979) describe a time-independent (spectral type) model based on a generalization of the "harmonic method" of Dronkers (1964) in which the current magnitude is represented through a truncated Taylor series that leads to a tractable representation of the friction term. Nonlinear terms are included in this method by means of an iteration procedure that updates the fundamental frequencies with contributions from the higher order harmonics.

Walters (1986) extended the work of Snyder and others (1979) by employing the finite-element method to their formulation. Simple linear triangular elements are used and shown to be sufficient in modeling simple problems.

Earlier works by Walters (1983) and Gray and Lynch (1979) show that spectral model solutions are free of spurious subgrid scale oscillations that commonly plague fully nonlinear formulations.

Kawahara and Hasegawa (1978) apply a completely different spectral approach in which Galerkin's method is used to integrate the shallow-water equations with respect to time. They assume that the tidal flow is periodic by applying trigonometric shape functions in time. In more recent papers, Kawahara and others (1981) extend this approach to two-layer flows.

In the model developed for this study, we focus only on the lowest order solution; that is, astronomical tides or tidal currents. The spectral model, at this level of approximation, is unable to resolve the overtides (or higher harmonics) which principally result from the nonlinear interaction between the tidal forcing and basin bathymetry. Higher order solutions are capable of resolving the higher harmonics or overtides of the principal tidal forcings.

MODEL FORMULATION

Linearizing the Shallow-Water Equations

The spectral model is based on the linearized shallow-water equations. Therefore, the spectral model inherits all the assumptions associated with the shallow-water equations. These equations describe gravity wave propagation in vertically well-mixed shallow embayments. We begin the formulation from the set of fully nonlinear shallow-water equations. For detailed descriptions of these equations and their underlying assumptions, see Dronkers (1964), Pritchard (1971), King and others, (1973), and La'Mehaute (1976).

The commonly used nonlinear, vertically averaged shallow-water equations are the continuity equation,

$$\frac{\partial \zeta}{\partial t} + \frac{\partial}{\partial x}(Hu) + \frac{\partial}{\partial y}(Hv) = 0, \qquad (1)$$

the x-momentum equation,

$$\frac{\partial u}{\partial t} + u\frac{\partial u}{\partial x} + v\frac{\partial u}{\partial y} = fv - g\frac{\partial \zeta}{\partial x} - \frac{gH}{2\rho_o}\frac{\partial \rho}{\partial x} + \frac{1}{\rho_o H}(\tau_x^s - \tau_x^b) + A_h\nabla^2 u, \qquad (2)$$

and the y-momentum equation,

$$\frac{\partial v}{\partial t} + u\frac{\partial v}{\partial x} + v\frac{\partial v}{\partial y} = -fu - g\frac{\partial \zeta}{\partial y} - \frac{gH}{2\rho_o}\frac{\partial \rho}{\partial y} + \frac{1}{\rho_o H}(\tau_y^s - \tau_y^b) + A_h\nabla^2 v, \qquad (3)$$

where

x,y = Cartesian coordinates in the horizontal plane;

t = time;

u,v = depth-averaged, tidal velocities in the x- and y-directions;

ζ = elevation of the water surface referenced to mean tide;

h = depth of basin below mean tide;

H = $h + \zeta$, total water depth;

ρ_o = reference density of water;

ρ = density of water;

τ_x^b = $gu\sqrt{(u^2+v^2)}C^{-2}$, the x-component of bottom stress;

τ_y^b = $gv\sqrt{(u^2+v^2)}C^{-2}$, the y-component of bottom stress;

τ_x^s = $C_d\rho_a w^2\sin\phi$, the x-component of wind stress;

τ_y^s = $C_d\rho_a w^2\cos\phi$, the y-component of wind stress;

C = Chezy friction coefficient;

C_d = drag coefficient for wind stress = 0.0026 (Smith and Cheng, 1987);

W = windspeed;

ϕ = wind direction measured clockwise from the positive y-axis;

A_h = horizontal eddy viscosity coefficient;

f = Coriolis parameter;

g = Acceleration due to gravity; and

∇^2 = The Laplacian operator.

These equations assume a hydrostatic pressure distribution and, following the Boussinesq approximation, use a reference density in all terms of the equations except the density-gradient terms in the momentum equations.

In linearizing the momentum equations, the terms that are underlined in equations 2 and 3 are dropped. The dropped terms include the advective acceleration terms, which become important in shallow areas and where rapid changes in bathymetry and diverging flows are being considered. Numerical experiments have shown the necessity of including advective acceleration terms in order to simulate large-scale eddying phenomena (Ponce and Yabusaki, 1980). The baroclinic terms $\frac{gH}{2\rho_o}\frac{\partial \rho}{\partial x}$ and $\frac{gH}{2\rho_o}\frac{\partial \rho}{\partial y}$ are linear terms, but they also are dropped in this formulation. These terms represent the lateral pressure gradient resulting from a horizontal density gradient. In situations where the freshwater inflow is a large percentage of the total tidal prism, these terms can be large and their omission can lead to errors in the computations. See Pritchard (1971) and Smith and Cheng (1987) for more information on baroclinic forcing. The horizontal momentum diffusion terms, $A_h \nabla^2 u$ and $A_h \nabla^2 v$, which in this case are based on an eddy-viscosity formulation (Schlichting, 1979; Tennekes and Lumley, 1972; and Rodi, 1984) also are dropped. From a dimensional analysis, these terms can be shown to be generally small; their omission will not greatly affect the computed results.

Following either the Chezy or Manning formulations (Chow, 1959; and White, 1979), friction is generally considered to be proportional to the square of the mean velocity. In the spectral model, however, the bottom stress is assumed to be a linear function of velocity,

$$\frac{1}{\rho_o H}(\tau_x^b) = \gamma u, \qquad \text{and} \qquad \frac{1}{\rho_o H}(\tau_y^b) = \gamma v,$$

where γ is a bottom stress coefficient.

Furthermore, the continuity equation is also linearized by assuming that the water-surface variations are small with respect to the mean depth ($\zeta << h$) and thus ($h \simeq H$).

After linearizing the continuity and momentum equations, the two-dimensional shallow-water equations become:

$$\frac{\partial \zeta}{\partial t} + \frac{\partial}{\partial x}(hu) + \frac{\partial}{\partial y}(hv) = 0 \qquad \text{(continuity)}, \tag{4}$$

$$\frac{\partial u}{\partial t} + g\frac{\partial \zeta}{\partial x} - fv + \gamma u = \left(\frac{\rho_a}{h\rho_o}\right) C_d W^2 \sin\phi \qquad \text{(x-momentum)}, \tag{5a}$$

$$\frac{\partial v}{\partial t} + g\frac{\partial \zeta}{\partial y} + fu + \gamma v = \left(\frac{\rho_a}{h\rho_o}\right) C_d W^2 \cos\phi \qquad \text{(y-momentum)}. \tag{5b}$$

Spectral Model Governing Equation

Assumption of Frequency Dependence

Assuming that the energy of the tides and the tidal currents reside in distinct packets or line spectra, the time dependence of these variables can be represented by the following summations of harmonic functions:

$$\zeta(x,y,t) = \sum_{n=1}^{N} Z_n(x,y)\cos[\omega_n t - \phi_n(x,y)] \tag{6a}$$

$$u(x,y,t) = \sum_{n=1}^{N} U_n(x,y)\cos[\omega_n t - \psi_n(x,y)] \tag{6b}$$

$$v(x,y,t) = \sum_{n=1}^{N} V_n(x,y)\cos[\omega_n t - \theta_n(x,y)] \tag{6c}$$

where

ω_n = angular speed (frequency) of the nth tidal constituent;

$Z_n(x,y)$ = water-surface amplitude for the nth tidal constituent;

$U_n(x,y), V_n(x,y)$ = amplitudes of the nth tidal constituent for velocity in the x,y directions;

$\phi_n(x,y)$ = phase lags for water-surface elevation for the nth tidal constituent;

$\psi_n(x,y), \theta_n(x,y)$ = phase lags for the u and v velocities, respectively, for the nth tidal constituent; and

N = number of tidal constituents.

The tidal frequencies ω_n are known from astronomical considerations, whereas the amplitudes for stage and velocity, Z_n, U_n, V_n, and their associated phases ϕ_n, ψ_n, θ_n, are the unknowns. The amplitudes and phases in equation 6 are known as harmonic constants. Once the harmonic constants are known, time series of tides and tidal currents can be computed using equation 6.

The expressions for ζ, and similarly for u and v can be written in complex notation as:

$$\zeta(x,y,t) = 1/2\{\sum_{n=1}^{N} [\zeta_n(x,y)\exp(-i\omega_n t) + \zeta_n^*(x,y)\exp(i\omega_n t)]\}, \quad (7a)$$

$$u(x,y,t) = 1/2\{\sum_{n=1}^{N} [u_n(x,y)\exp(-i\omega_n t) + u_n^*(x,y)\exp(i\omega_n t)]\}, \quad (7b)$$

$$v(x,y,t) = 1/2\{\sum_{n=1}^{N} [v_n(x,y)\exp(-i\omega_n t) + v_n^*(x,y)\exp(i\omega_n t)]\}, \quad (7c)$$

ζ_n, u_n, and v_n are complex variables that are functions of both the amplitude and phase of the nth component shown in equation 6. These variables commonly are called modal quantities because they represent the nth frequency or the nth mode of a given tidal forcing. The ζ_n^*, u_n^*, v_n^* quantities represent the complex conjugates of ζ_n, u_n, and v_n, respectively.

The governing equation of the spectral model is obtained for the nth tidal frequency by substituting equation 7 into the linearized shallow-water equations 4 and 5. The resulting equations are multiplied by $\exp(^{-i\omega_n t})$ which produces a final equation set with both real and imaginary components. When these equations are arranged to equal zero, both the imaginary and real parts of the equation must be identically equal zero. Fortunately, the real and imaginary parts yield equivalent expressions; thus, the solution of either is sufficient. The real portion of these relations yield:

$$-i\omega_n\zeta_n + \frac{\partial}{\partial x}(hu_n) + \frac{\partial}{\partial y}(hv_n) = 0 \qquad \text{(continuity)}, \quad (8)$$

$$-i\omega_n u_n + g\frac{\partial \zeta_n}{\partial x} - fv_n + \gamma_n u_n = (W_s/h)\sin\phi \qquad \text{(x-momentum)}, \quad (9)$$

$$-i\omega_n v_n + g\frac{\partial \zeta_n}{\partial y} + fu_n + \gamma_n v_n = (W_s/h)\cos\phi \qquad \text{(y-momentum)}, \quad (10)$$

where

$$W_s = \delta(\omega_n)(\rho_a/\rho_o)C_d W^2,$$

and $\delta(\omega_n)$ is a dirac delta function such that

$$\delta(\omega_n) = 1, \quad \text{if } \omega_n = 0,$$

$$\delta(\omega_n) = 0, \quad \text{if } \omega_n \neq 0.$$

The wind stress is incorporated into the spectral model only in the zero frequency mode. Wind forcing is placed in the zero frequency because the wind, in general, is not correlated with any given astronomical frequency. An extension to variable wind is possible, but is beyond the scope of the present discussion.

The above relations (equations 8, 9, and 10) are derived for the nth frequency where the complete solution results from superposition of all N frequencies indicated by the summations in equation 6.

The velocities, u_n and v_n, are solved from the momentum equations in terms of ζ_n as

$$u_n = -\left(\frac{gq_n}{q_n^2+f^2}\right)\frac{\partial \zeta_n}{\partial x} - \left(\frac{fg}{q_n^2+f^2}\right)\frac{\partial \zeta_n}{\partial y} + W_x /h, \tag{11}$$

$$v_n = -\left(\frac{gq_n}{q_n^2+f^2}\right)\frac{\partial \zeta_n}{\partial y} + \left(\frac{fg}{q_n^2+f^2}\right)\frac{\partial \zeta_n}{\partial x} + W_y /h, \tag{12}$$

where

$$q_n = -i\omega_n + \gamma_n, \tag{13}$$

$$W_x = \left(\frac{W_s}{q_n^2+f^2}\right)(f\cos\phi + q_n \sin\phi), \tag{14}$$

$$W_y = \left(\frac{W_s}{q_n^2+f^2}\right)(q_n\cos\phi - f\sin\phi). \tag{15}$$

In equations 11 and 12, the coefficients of $\partial\zeta_n/\partial x$ and $\partial\zeta_n/\partial y$ are constants for each frequency, and the wind stress must be specified. Therefore, the modal velocities u_n, v_n are functions of the modal water-surface gradients alone.

Finally, by substituting u_n and v_n from equations 11 and 12 into equation 8, the governing equation for the modal water-surface elevation is given as:

$$i\omega_n\zeta_n + \nabla\cdot[gh(\frac{q_n}{q_n^2+f^2})\nabla\zeta_n] + fg\{\frac{\partial}{\partial x}[(\frac{h}{q_n^2+f^2})\frac{\partial\zeta_n}{\partial y}] - \frac{\partial}{\partial y}[(\frac{h}{q_n^2+f^2})\frac{\partial\zeta_n}{\partial x}]\} =$$

$$\frac{\partial}{\partial x}(W_x) + \frac{\partial}{\partial y}(W_y), \qquad (16)$$

where the $\nabla(\ )$ is the gradient operator and the $\nabla\cdot(\ )$ is the divergence operator. The notation in equation 16 can be greatly simplified by denoting

$$D_{xx} = D_{yy} = gh(\frac{q_n}{q_n^2+f^2}) \qquad (17a)$$

$$D_{xy} = -D_{yx} = gh(\frac{f}{q_n^2+f^2}) \qquad (17b)$$

and defining a second rank tensor, $\underline{\underline{D}}$ as

$$\underline{\underline{D}} = \begin{vmatrix} D_{xx} & D_{xy} \\ D_{yx} & D_{yy} \end{vmatrix}$$

Equation 16 in vectorial form is a complex Helmholtz equation,

$$i\omega_n\zeta_n + \nabla\cdot(\underline{\underline{D}}\nabla\zeta_n) = \frac{\partial}{\partial x}(W_x) + \frac{\partial}{\partial y}(W_y), \qquad (18)$$

for the complex modal water-surface elevation. Equation 18, which is time independent and involves one unknown, ζ_n, determines the spatial variation in the modal water surface elevation for frequency ω_n. The solution of equation 18 for ζ_n gives both the amplitude and phase distributions of the tidal elevation for the nth constituent.

Once ζ_n becomes known and its gradients determined, the modal velocities are calculated using equations 11 and 12. Finally, after ζ_n, u_n, and v_n have been calculated for all desired astronomical frequencies using equations 11, 12, and 18, the linear combination of the solution for each frequency gives the

instantaneous solutions for ζ, u, and v. Thus, equation 18 represents the basic governing equation of the problem; calculation of the modal velocities from equations 11 and 12 and the time-dependent values of the tides and tidal currents as given in equation 6 are merely subsequent calculations that do not affect the solution.

METHOD OF SOLUTION

Method of Weighted Residuals--Galerkin Method

Although there are many varied approaches to obtain numerical solutions of boundary value problems involving equation 18, these methods generally can be divided into two major categories: (1) finite-difference methods and (2) finite-element methods. Every numerical technique has certain strengths and weaknesses which need to be weighed against the nature of the differential equation and the specific problem being solved. In general, for the finite-element method, the computational grids are not regular, and the strength of the finite-element method resides in its ability to accommodate the placement of the computational emphasis where it is needed or desired. Because tidal current is strongly controlled by bathymetry, the advantages associated with being able to accurately define the basin geometry using the finite-element method suggest the use of this approach over the use of the finite-difference method.

The following sections provide a brief outline of the finite-element method applied to the spectral model governing equation. By applying the finite-element method, the governing partial differential equation is transformed into a matrix equation that can be solved using a standard matrix solver. Although most of this material can be found in texts on the finite-element method, it is provided in this report for completeness and as a prelude to discussion of the specific formulation of the boundary conditions in this model. This section covers the concepts of weighted residuals, weighting functions, and element shape functions. Some terms in the governing equations either are rearranged into forms suitable for inclusion in the computer code or

need specific modification to treat different boundary conditions, such as parallel flow or flux conditions including wind. For further reading on finite elements and further detailed explanation of certain topics in the following sections, see Huebner (1975), Pinder and Gray (1977), Cheng (1978), and Zienkiewicz (1979).

The ultimate goal of any numerical solution scheme is to represent, in a discrete sense, the continuum response to a given governing equation subject to certain boundary conditions, such as the classic boundary value problem. In the spectral model we seek the solution, ζ_n, to equation 18 at discrete locations known as nodes. Introducing an approximate solution $\bar{\zeta}_n$ for ζ_n in equation 18 gives

$$i\omega_n\bar{\zeta}_n + \nabla\cdot(\underline{D}\nabla\bar{\zeta}_n) - W_d = R \tag{19}$$

where

$$W_d = \frac{\partial}{\partial x}(W_x) + \frac{\partial}{\partial y}(W_y),$$

and R is the error, or residual, that results from the substitution of the approximate solution $\bar{\zeta}_n$ in equation 18. As the approximate solution $\bar{\zeta}_n$ approaches the exact solution, ζ_n, the residual, R, approaches zero. The finite-element method, therefore, seeks to force the residuals to zero, in some sense, so that the errors introduced by the approximate solution are minimized and spread over the entire domain. To distribute these errors over the entire domain we select a set of P linearly independent weighting functions, (W), and then require that the weighted average of the residuals tend to zero as expressed by the following relation:

$$\int_\Omega W_k R \, d\Omega = 0, \qquad k = 1,2,3....P \tag{20}$$

where the integral in this expression is applied over the entire solution domain, Ω. Integration over the entire domain is accomplished by performing individual integrations over M subregions, $\Omega^{(I)}$, I=1,2....M called elements so that

$$\int_\Omega W_k R \, d\Omega \simeq \sum_{I=1}^{M} \left[\int_{\Omega(I)} W_k R \, d\Omega^{(I)}\right], \qquad k = 1,2,..... P. \tag{21}$$

Consider a typical finite-element mesh (fig. 1) where the domain is subdivided into a number of triangular elements. Although the elements can be any polygon, we use triangles here for simplicity and to be consistent with the final selection and use of triangular elements in the computer code. A typical element is defined by the node numbers i,j,k where the coordinates of the vertices are x_i,y_i, x_j,y_j, and x_k,y_k, respectively.

If the approximate solutions, $\bar{\zeta}_n$, are defined in each subregion or element as $\bar{\zeta}_n^{(I)}$, then the approximate solution, $\bar{\zeta}_n$, for the entire domain is the union of all the elemental solutions $\bar{\zeta}_n^{(I)}$ with the requirement that the boundary joining neighboring elements be continuous and have, at least, piecewise continuous first-order derivatives. This is known in the literature as C-zero order continuity or C^0 continuity.

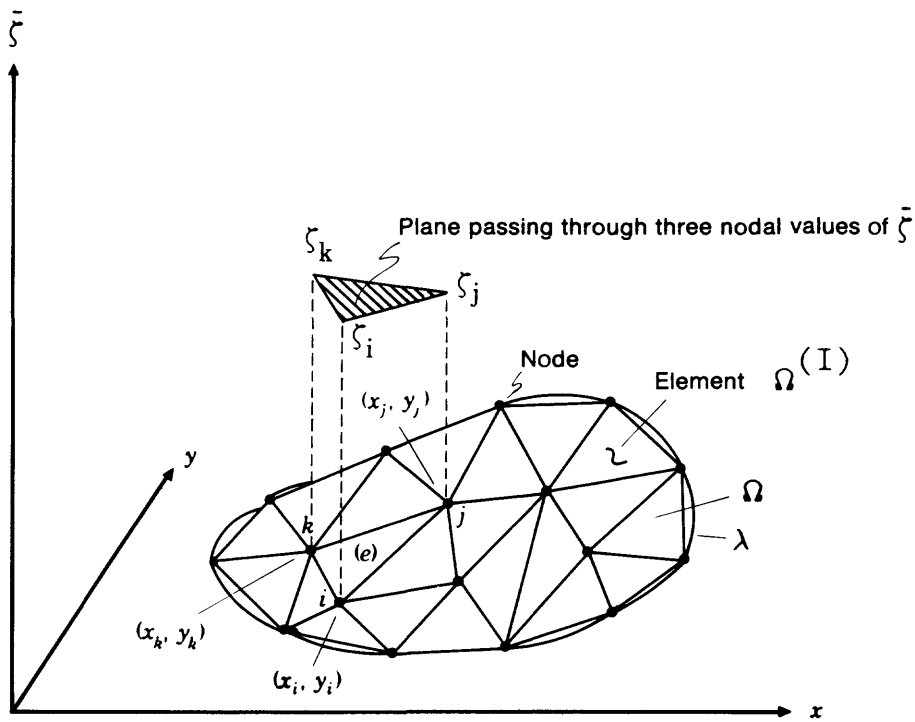

FIGURE 1. – Subdivided domain Ω and piecewise linear solution surface, $\bar{\zeta}(x, y)$.

A graphical representation of the approximate solution defined on an element is shown in figure 2. The elemental solution in figure 2 is a plane which results from choosing linear triangles as the element type. The approximate solution $\bar{\zeta}_n$ in the individual subdomain or element $\Omega^{(I)}$ is defined as:

$$\bar{\zeta}_n^{(I)}(x,y) = \zeta_{n_i} N_i^{(I)}(x,y) + \zeta_{n_j} N_j^{(I)}(x,y) + \zeta_{n_k} N_k^{(I)}(x,y) \tag{22}$$

where the N's represent shape functions and the superscripts indicate that the shape functions are defined over the element $\Omega^{(I)}$ only. The top picture in figure 2 graphically depicts this mathematical form of the elemental solution. The lower three figures represent the functions, $N_i^{(I)}$, $N_j^{(I)}$, and $N_k^{(I)}$ called shape functions, defined at each of the nodes. The shape functions have the property of retaining a value of 1 at the node where it is defined and zero at the other nodes in the element. Mathematically this property is described by the Kronecker delta, $N_i(x_j,y_j) = \delta_{i,j}$. Furthermore, the shape functions for a given element are zero everywhere except in that element. In other words, $N_i^{(I)}(x,y) = 0$, if $(x,y) \notin \Omega^{(I)}$. This property results in the final system of equations being banded.

Depending on the choice of weighting functions in equation 20, specific weighted residual techniques are (Pinder and Gray, 1977): (1) subdomain method, (2) collocation method, (3) least-squares method, (4) method of moments, and (5) Galerkin's method. Galerkin's method is considered the most general formulation and is the method applied in this report. In Galerkin's method, the weighting functions are selected to be the same as the shape functions, N_k.

With the weighting functions chosen to be the same as the shape functions, that is:

$$W_k = N_k \tag{23}$$

equation 20 becomes,

$$\sum_{I=1}^{M} \left[\int_{\Omega^{(I)}} N_k [i\omega_n \bar{\zeta}_n + \nabla \cdot (\underline{\underline{D}} \nabla \bar{\zeta}_n) - W_d] \, d\Omega^{(I)} = 0. \right.$$

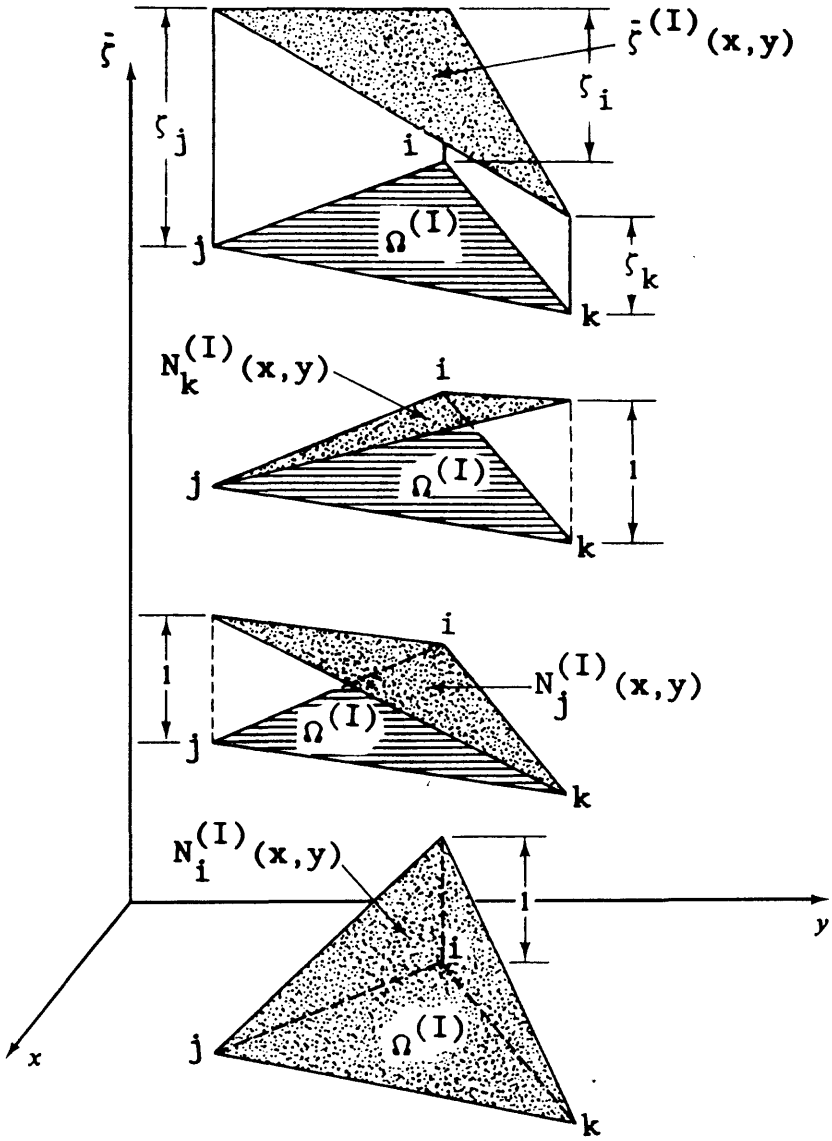

$$\bar{\zeta}_n^{(I)}(x,y) = \zeta_{n_i} N_i^{(I)}(x,y) + \zeta_{n_j} N_j^{(I)}(x,y) + \zeta_{n_k} N_k^{(I)}(x,y)$$

FIGURE 2. – Linear shape functions $N_i^{(I)}$ over a triangular element $\Omega^{(I)}$ and their linear combination.

or,

$$\sum_{I=1}^{M} [i\omega_n \int_{\Omega(I)} N_k d\Omega^{(I)} + \int_{\Omega(I)} N_k \nabla\cdot(\underline{\underline{D}}\nabla\bar{\zeta}_n) d\Omega^{(I)} - \int_{\Omega(I)} N_k W_d d\Omega^{(I)}] = 0. \quad (24)$$

(1) (2) (3)

The first and third terms in equation 24 can be easily evaluated; therefore, the following section will expand only the second term. By applying the following identity to reduce the order of differentiation (that is, a reduction of a second-order partial differential equation into the product of two first-order derivatives),

$$N_k \nabla\cdot(\underline{\underline{D}}\nabla\bar{\zeta}_n) = \nabla\cdot(N_k \underline{\underline{D}}\nabla\bar{\zeta}_n) - \nabla N_k \cdot \underline{\underline{D}}\nabla\bar{\zeta}_n , \quad (25)$$

the second term in equation 24 becomes,

$$\int_{\Omega(I)} N_k \nabla\cdot(\underline{\underline{D}}\nabla\bar{\zeta}_n) d\Omega^{(I)} = \int_{\Omega(I)} \nabla\cdot(N_k \underline{\underline{D}}\nabla\bar{\zeta}_n) d\Omega^{(I)} - \int_{\Omega(I)} \nabla N_k \cdot \underline{\underline{D}}\nabla\bar{\zeta}_n \, d\Omega^{(I)}. \quad (26)$$

In order to apply Nuemann-type boundary conditions, the first term on the right-hand side of equation 26 is further reduced by Green's theorem to give

$$\int_{\Omega(I)} N_k \nabla\cdot(\underline{\underline{D}}\nabla\bar{\zeta}_n) d\Omega^{(I)} = \int_{\lambda(I)} (N_k \underline{\underline{D}}\nabla\bar{\zeta}_n) \vec{\eta} d\lambda^{(I)} - \int_{\Omega(I)} \nabla N_k \cdot \underline{\underline{D}}\nabla\bar{\zeta}_n \, d\Omega^{(I)} \quad (27)$$

where $\lambda^{(I)}$ represents the boundary of the element, and $\vec{\eta}$ is the unit outward-pointing unit normal to $\lambda^{(I)}$.

After these analytical treatments, the governing equation of the spectral model becomes:

$$\sum_{I=1}^{M} [i\omega_n \int_{\Omega(I)} N_k d\Omega^{(I)} - \int_{\Omega(I)} \nabla N_k \cdot \underline{\underline{D}}\nabla\bar{\zeta}_n \, d\Omega^{(I)} + \int_{\lambda(I)} (N_k \underline{\underline{D}}\nabla\bar{\zeta}_n) \vec{\eta} d\lambda^{(I)} - \int_{\Omega(I)} N_k W_d d\Omega^{(I)}] = 0. \quad (28)$$

Equation 22 can be rewritten in matrix form, with the x,y dropped for clarity:

$$\bar{\zeta}_n^{(I)} = [\, N_i^{(I)} \; N_i^{(I)} \; N_i^{(I)} \,] \begin{Bmatrix} \zeta_{n_i} \\ \zeta_{n_j} \\ \zeta_{n_k} \end{Bmatrix}$$

or, more compactly yet,

$$\bar{\zeta}_n = [N]\{\zeta_n\}, \tag{29}$$

where the notations [ ] and { } represent row and column vectors respectively. Because the superscript (I) has been dropped, we make the assumption that $\bar{\zeta}_n$ and the integrals in equation 28 now represent the solution for the nth frequency on any arbitrary element within the domain. Substituting equation 29 into equation 28, applying indicial notation [where (x_1,x_2) are (x,y)] using the summation convention, and expanding the divergence and gradient operators, equation 28 can be rewritten in vector form as:

$$i\omega_n \int_\Omega \{N\}[N]\{\zeta_n\}\, d\Omega - \int_\Omega D_{i,j} \frac{\partial\{N\}}{\partial x_i} \frac{\partial\{N\}}{\partial x_j}\{\zeta_n\}\, d\Omega + \int_\lambda \{N\}\{\eta_i\} D_{i,j} \frac{\partial \zeta_n}{\partial x_j}\, d\lambda = \int_\Omega \{N\} W_d d\Omega \tag{30}$$

where the i,j=1,2 represent the x and y coordinate directions respectively, and η_1, η_2 represent the tangential and unit outward pointing normals respectively.

Because $D_{i,j}$ is specified at the nodes and can vary at each node within an element, two approaches are possible in representing this function. One method assumes a constant value of $D_{i,j}$ within an element obtained through averages of the nodal $D_{i,j}$ values. A second approach assumes that the tensor $D_{i,j}$ varies within the element according to the shape functions such that

$$D_{i,j}(x,y) = [D_{i,j}]\{N\}. \tag{31}$$

In order to keep the analysis general, the latter method, which accounts for variations of $D_{i,j}$ within the element, will be applied. However, the two approaches are identical if simple (linear) triangular shape functions are used in equation 31 and an arithmetic average is applied in the first approach.

With the above substitution for $D_{i,j}$, equation 30 becomes:

$$i\omega_n \int_\Omega \{N\}[N]\{\zeta_n\}\, d\Omega - \int_\Omega [D_{i,j}]\{N\}\frac{\partial\{N\}}{\partial x_i}\frac{\partial\{N\}}{\partial x_j}\{\zeta_n\}\, d\Omega + \int_\lambda \{N\}\{\eta_i\}D_{i,j}\frac{\partial \zeta_n}{\partial x_j}\, d\lambda = \int_\Omega \{N\}W_d d\Omega. \quad (32)$$

Further modifications of equation 32 are necessary to apply the boundary conditions in the model.

Shape Function Selection

Because this model is based on the linearized shallow-water equations, the philosophy behind element selection was one of simplicity. Thus, triangular elements are used in this model. Linear elements have a planar functional mapping of the unknowns within each element. Because of this property, the first-order partial derivatives (gradients) of the solution variable(s) are constant within each element, and higher order derivatives are not defined.

Because the modal velocities are strictly functions of the gradients of ζ_n, velocities are constant within linear elements. As a result, the velocities in this model are assumed to be spatially coincident with the element centroid.

Boundary Conditions

Three types of boundary conditions can be invoked in this model: (1) Parallel flow condition which ensures the conservation of mass at the shoreline boundaries, (2) the specification of velocities on the boundary (open boundary condition), and (3) the specification of the dependent variable ζ_n anywhere in the domain, including points on the boundary.

Shoreline Boundaries

Two types of closed boundary conditions can be applied at the shoreline boundary. The first is a no-slip condition wherein the velocities in the elements adjacent to the shoreline boundary are forced to zero. This approach is sometimes considered too stringent when the element size is much larger than the boundary layer associated with a solid boundary. A less restrictive boundary condition that forces the velocity to be parallel to the shoreline boundary is used in this and many other models.

For each mode, n, the parallel flow condition implies

$$\eta_1 u_n + \eta_2 v_n = 0, \tag{33}$$

where η_1, η_2 are direction cosines of the outward pointing unit normal to the boundary in the x_1 and x_2 directions, respectively (fig. 3). Substituting the expressions for u_n and v_n from equations 11 and 12 into equation 33 and rearranging terms, the parallel flow condition becomes

$$q_n\left[\eta_1\frac{\partial \zeta_n}{\partial x_1} + \eta_2\frac{\partial \zeta_n}{\partial x_2}\right] + f\left[\eta_1\frac{\partial \zeta_n}{\partial x_2} - \eta_2\frac{\partial \zeta_n}{\partial x_1}\right] = \frac{\eta_1 W_s}{hg}(f\cos\phi + q_n\sin\phi) + \frac{\eta_2 W_s}{hg}(q_n\cos\phi - f\sin\phi).$$

In order to implement this boundary condition, it is desirable to transform this equation into a local coordinate system, ν,τ, aligned with the outward pointing unit normal to the boundary (fig. 4). By definition,

$$\eta_1\frac{\partial \zeta_n}{\partial x_1} + \eta_2\frac{\partial \zeta_n}{\partial x_2} = \frac{\partial \zeta_n}{\partial \nu}$$

and,

$$\eta_1\frac{\partial \zeta_n}{\partial x_2} - \eta_2\frac{\partial \zeta_n}{\partial x_1} = \frac{\partial \zeta_n}{\partial \tau}$$

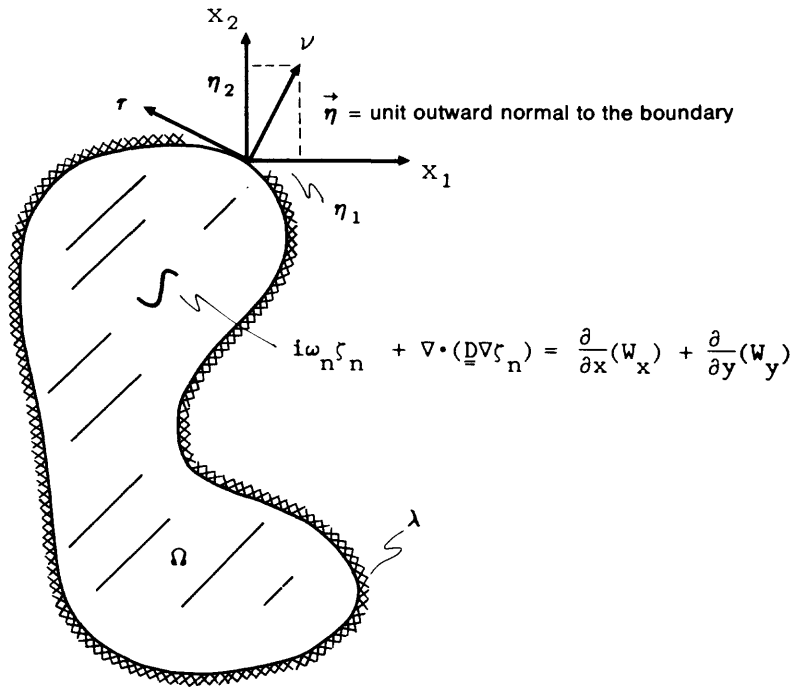

FIGURE 3. – Definition of coordinates. The Helmholtz equation is applied throughout the domain Ω. The unit outward normal $\vec{\eta}$ is defined on the domain boundary λ where $\vec{\eta}$ can be represented by the direction cosines η_1, η_2 and $\vec{\tau}$ represents the unit tangent vector to the boundary.

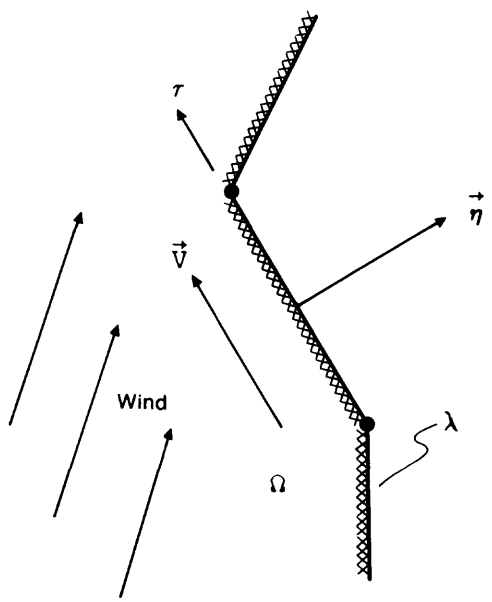

FIGURE 4. – Example of the parallel flow condition applied to a boundary segment where $\vec{V}$ represents the velocity of the water. When the inner product of $\vec{\eta}$ and $\vec{V}$ is forced to zero, $\vec{V}$ will be parallel to $\vec{\tau}$.

where ν is the normal direction (positive outward) and τ the tangential direction (positive in the direction rotated 90 degrees counterclockwise to the outward pointing unit normal). With this coordinate transform, the parallel flow condition becomes:

$$q_n \frac{\partial \zeta_n}{\partial \nu} = -f \frac{\partial \zeta_n}{\partial \tau} + \frac{\eta_1 W_s}{hg}(f\cos\phi + q_n \sin\phi) + \frac{\eta_2 W_s}{hg}(q_n \cos\phi - f\sin\phi). \tag{34}$$

The parallel flow condition is invoked in the model through the line integral applied in equation 32. Before applying equation 34 as the parallel flow condition, the line integral is rewritten in ν,τ coordinates through the following matrix operations,

$$\int_\lambda \{N\}\eta_i D_{i,j} \frac{\partial \zeta_n}{\partial x_j} d\lambda = \int_\lambda \{N\}\eta_i D_{i,j} \underline{\underline{A}}^{-1} \underline{\underline{A}} \frac{\partial \zeta_n}{\partial x_j} d\lambda, \tag{35}$$

where the matrix $\underline{\underline{A}}$ is a known matrix which performs a coordinate rotation into the (ν,τ) axes, with

$$\underline{\underline{A}} = \begin{bmatrix} \eta_1 & \eta_2 \\ -\eta_2 & \eta_1 \end{bmatrix} \quad \text{and} \quad \underline{\underline{A}}^{-1} = \begin{bmatrix} \eta_1 & -\eta_2 \\ \eta_2 & \eta_1 \end{bmatrix}$$

Furthermore, $\eta_1^2 + \eta_2^2 = 1$, and

$$\underline{\underline{A}} \frac{\partial \zeta_n}{\partial x_j} = \begin{Bmatrix} \frac{\partial \zeta_n}{\partial \nu} \\ \frac{\partial \zeta_n}{\partial \tau} \end{Bmatrix}$$

and

$$\eta_i D_{i,j} \underline{\underline{A}}^{-1} = [D_\nu \; D_\tau],$$

where

$$D_\nu = \eta_1^2 D_{11} + \eta_1\eta_2 D_{21} + \eta_1\eta_2 D_{12} + \eta_2^2 D_{22},$$

$$D_\tau = -\eta_1\eta_2 D_{11} - \eta_2^2 D_{21} + \eta_1^2 D_{12} + \eta_2\eta_1 D_{22}.$$

The second rank tensor, $\underline{D}$, defined in equation 17, is anti-symmetric, where $D_{22} = D_{11}$ and $D_{21} = -D_{12}$. It follows from the above equations that D_ν and D_τ become

$$D_\nu = D_{11} \qquad \text{and} \qquad D_\tau = D_{12}.$$

Using the above relations, equation 35 is transformed into the ν,τ coordinates,

$$\int_\lambda \{N\}\eta_i D_{i,j} \frac{\partial \zeta_n}{\partial x_j}\, d\lambda = \int_\lambda \{N\}[D_{11} \frac{\partial \zeta_n}{\partial \nu} + D_{12} \frac{\partial \zeta_n}{\partial \tau}]\, d\lambda. \tag{36}$$

Finally, substituting equation 34 into equation 36 for $\frac{\partial \zeta_n}{\partial \nu}$ gives

$$\int_\lambda \{N\}\eta_i D_{i,j} \frac{\partial \zeta_n}{\partial x_j}\, d\lambda = \int_\lambda \{N\}(D_{11}/q_n)[-f \frac{\partial \zeta_n}{\partial \tau} + \frac{\eta_1 W_s}{hg}(f\cos\phi + q_n \sin\phi)$$

$$+ \frac{\eta_2 W_s}{hg}(q_n \cos\phi - f\sin\phi)]\, d\lambda + \int_\lambda \{N\}[D_{12} \frac{\partial \zeta_n}{\partial \tau}]\, d\lambda.$$

The product of $(f/q_n)D_{11}$ is identically equal to D_{12}; therefore the $\frac{\partial \zeta_n}{\partial \tau}$ terms cancel. This implies that the parallel flow condition without wind stress is simply the natural boundary condition

$$\int_\lambda \{N\}\eta_i D_{i,j} \frac{\partial \zeta_n}{\partial x_j}\, d\lambda = 0.$$

The parallel flow condition with wind can be expressed as

$$\int_\lambda \{N\}\eta_i D_{i,j} \frac{\partial \zeta_n}{\partial x_j}\, d\lambda = \int_\lambda \{N\}(\eta_1\{W_x\} + \eta_2\{W_y\})\, d\lambda.$$

where $\{W_x\}$ and $\{W_y\}$ are given in equations 14 and 15.

Open Boundaries--Velocity Specification

Tidal velocities and net tributary discharges can be specified as model boundary conditions. Similar to the parallel flow condition, velocities are invoked in the model through the line integral in equation 32. Equations 11 and 12 are rearranged so that the modal water-surface gradients are written in terms of velocity components as:

$$\frac{\partial \zeta_n}{\partial x} = 1/g(fv - q_n u + \frac{W_s}{h}\sin\phi) \qquad \text{(x-momentum)}, \qquad (37)$$

$$\frac{\partial \zeta_n}{\partial y} = 1/g(-fu - q_n v + \frac{W_s}{h}\cos\phi) \qquad \text{(y-momentum)}. \qquad (38)$$

where u and v are specified as boundary conditions. Substituting equations 37 and 38 into the line integral in equation 32 gives the following result after some rearrangement,

$$\int_\lambda \{N\}\eta_i D_{i,j} \frac{\partial \zeta_n}{\partial x_j} d\lambda = [h(\eta_1 u + \eta_2 v) - W_B] \int_\lambda \{N\} d\lambda, \qquad (39)$$

where the contribution from the wind to the flux boundary condition, W_B, is

$$W_B = (\frac{W_s}{q_n^2+f^2})[q_n\eta_1 - f\eta_2)\sin\phi + (f\eta_1 + q_n\eta_2)\cos\phi],$$

and the quantity $(\eta_1 u + \eta_2 v)$ represents the component of any arbitrarily specified velocity u and v in the unit outward pointing normal direction.

Open Boundaries--Level Specification

Previous sections have indicated how flux and parallel flow conditions (Neumann-type boundary conditions) are handled in the model; as shown, these boundary conditions can be applied only after some analytical manipulation of the governing equations. Another type of boundary condition, where the solution variables are specified at the nodes, remains to be discussed. This is a Dirichlet boundary condition which is used to define the water-surface amplitude, ζ_n, at the open boundaries and at points within the domain. When stage data are available for a given study area, Dirichlet boundary conditions can be used to force the solution to exactly match the stage data at the corresponding locations in the model. Dirichlet boundary conditions are applied in the model by modifying the solution matrices.

Matrix Representation of Governing Equation

In matrix form, equation 32 can be rewritten as:

$$([A] - [B])\{\zeta_n\} = -\{C\} + \{E\} - \{G\}. \tag{40}$$

where the matrices [A] and [B] are evaluated within the domain as

$$[A] = i\omega_n \int_\Omega \{N\}[N]\, d\Omega,$$

and

$$[B] = \int_\Omega [D_{i,j}]\{N\}\frac{\partial\{N\}}{\partial x_i}\frac{\partial\{N\}}{\partial x_j}\, d\Omega.$$

$\{C\}$ enables the prescription of velocities along segment boundaries where

$$[C] = \{h(\eta_1 \mathbf{u} + \eta_2 \mathbf{v}) - W_B\} \int_\lambda \{N\} d\lambda,$$

Finally, $\{E\}$ and $\{G\}$ are related to the wind stress forcing such that

$$\{E\} = \int_\Omega \{N\}\frac{\partial[N]}{\partial x}\{W_x\} d\Omega + \int_\Omega \{N\}\frac{\partial[N]}{\partial y}\{W_y\} d\Omega,$$

and

$$\{G\} = \int_\lambda \{N\}(\eta_1 W_x + \eta_2 W_y)\, d\lambda,$$

The resultant of the matrices ([A] - [B]) is commonly referred to as the stiffness matrix and the expression $(-\{C\} + \{E\} - \{G\})$ is known as the load vector. If linear elements are used, W_x and W_y in the vectors $\{E\}$, $\{G\}$ and $\{C\}$ take on values specified at the nodes.

The $D_{i,j}$'s in vector {C} require some additional comment. The $D_{i,j}$ at the boundary nodes can be zero because the mean depth, h, can be specified as zero there; however, the $D_{i,j}$ within the element will not be zero. If linear triangular elements are used in this analysis, then the velocities within the element are constant and are assumed to coincide with the center of the element. Thus, the nodal average of the $D_{i,j}$'s must be used in vector {C} to enforce the specified velocity in the boundary elements.

NUMERICAL EXPERIMENTS

In this section, spectral model results for two separate problems involving identical geometries are compared with analytical solutions described by Lynch and Gray (1979). The numerical experiments were made using a rectangular basin with planar dimensions of 91.44 by 121.92 km with an undisturbed water depth of 12.192 m as shown in figure 5. The top, bottom, and left- hand side of this basin are closed to mass flux while the right-hand side is an open boundary. The finite-element grid used in the numerical experiments also is depicted in figure 5. In both experiments Coriolis forcing was not modeled, and a constant bottom friction $\gamma_n = 0.0001$ was used.

In the first numerical experiment, stage, in meters, is specified on the open boundary such that $\zeta = (0.03048)\cos\omega t$ where $\omega = 2\pi/T$ and T is the M2 tidal period of 12.4 hours. Results between the analytical solution and model results compare favorably as shown in figures 6*A* and 6*B*.

The second problem uses the same geometry and finite-element grid as the first problem, except that a zero amplitude stage is specified on the open boundary and a constant 5.5 m/s wind is applied over the entire domain in the negative x-direction. Model results compare almost identically with analytical solutions for sea level as shown in figure 6*C*. Velocities for both the analytical solution and the model were zero for the second problem.

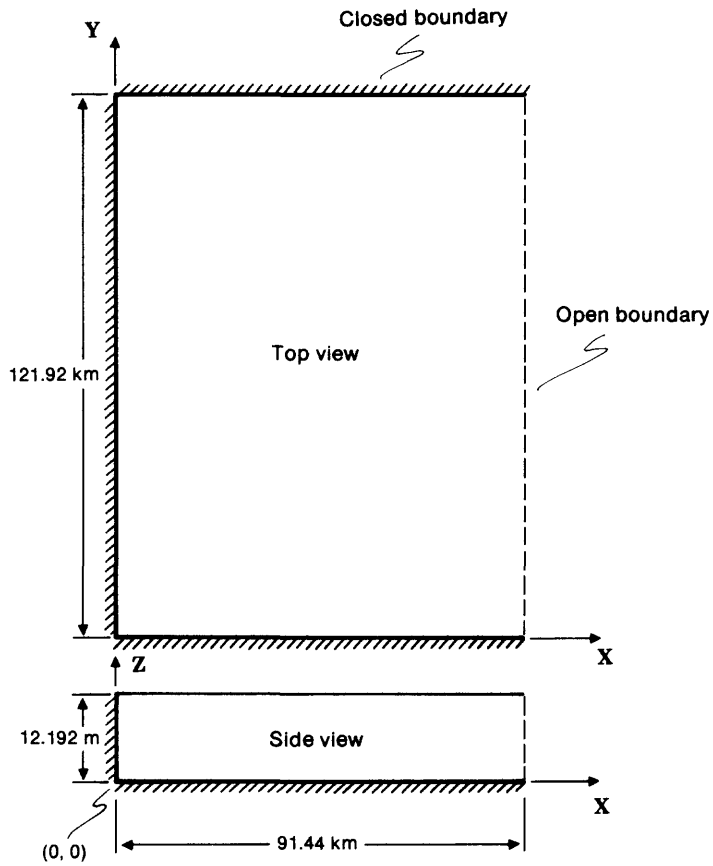

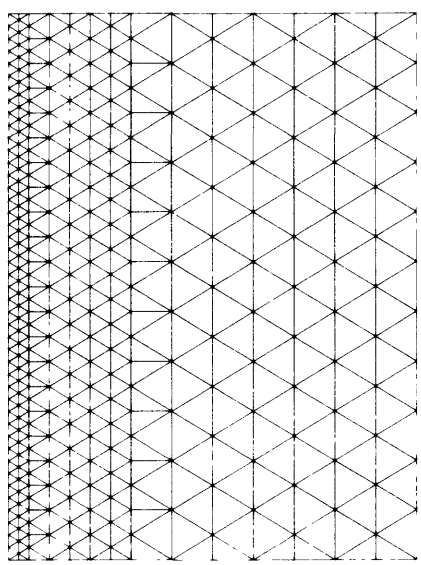

Finite-element grid

FIGURE 5.—Geometry and finite-element grid used in numerical experiments.

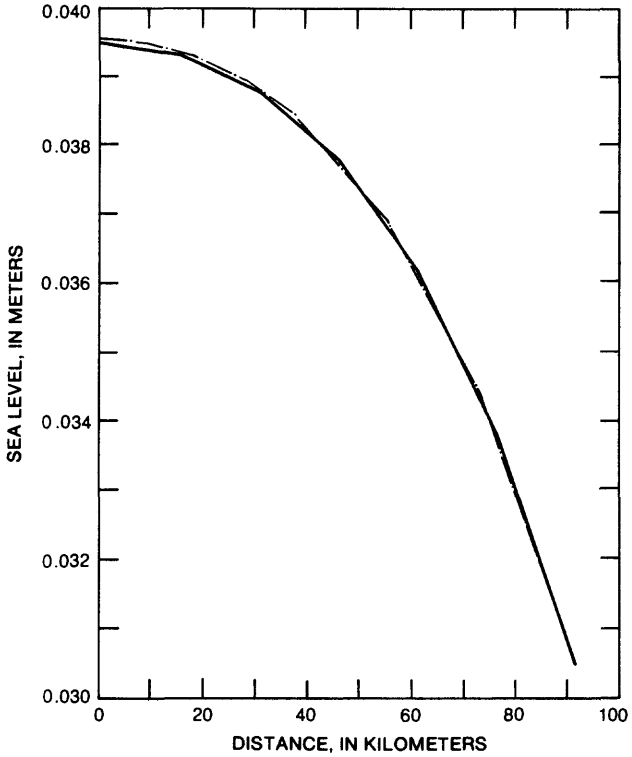

A, Sea-level comparison. Stage specified along the open boundary.

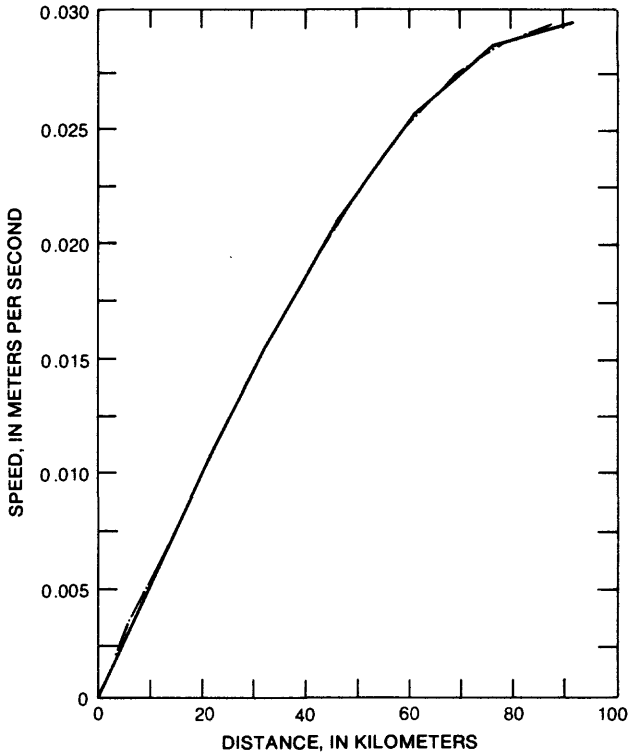

B, Current speed comparison. Stage specified along the open boundary.

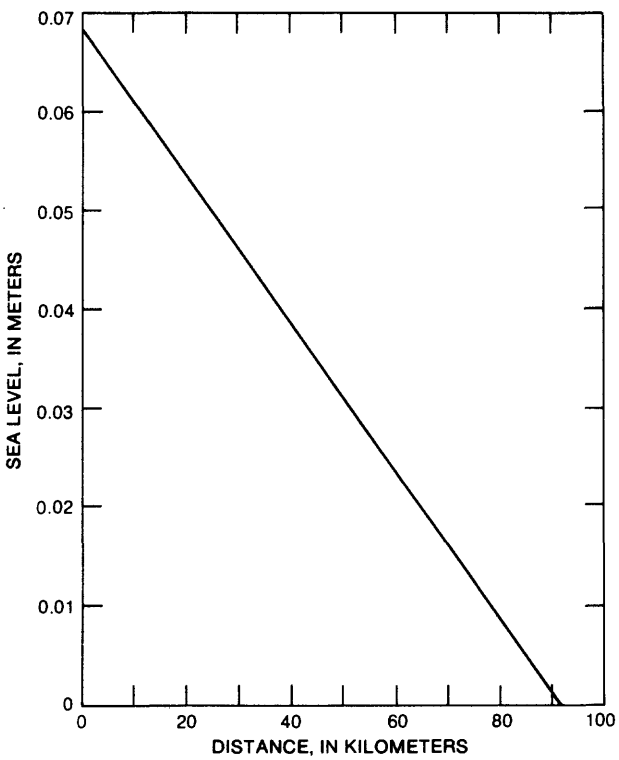

C, Sea-level comparison using a 5.5 meter-per-second wind applied in the negative x-direction.

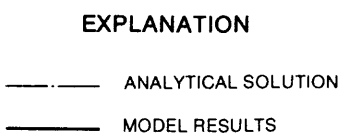

FIGURE 6. Comparisons between analytical and model results.

CONCLUSIONS

This report discusses the formulation, assumptions, and the strengths and weaknesses of a spectral model based on the linearized shallow-water equations. The spectral model solution method is an efficient algorithm designed specifically to handle tidal circulation dominated by astronomical forcing in complex embayments where the nonlinear effects are assumed small or unimportant. The efficiency of this method is achieved through a transformation of the governing equations into the frequency domain. With this transformation, the resulting governing equation takes the form of the classic Helmholtz equation that can be solved for the modal (or complex) water-surface amplitudes and phases. Once the distribution of the water-surface amplitudes for a given frequency is calculated from the Helmholtz equation, the modal velocities are evaluated using the momentum equations. The final instantaneous values for the water-surface elevations and velocities can be obtained subsequently by evaluation of simple algebraic expressions. Because of the simplicity of the calculations for the instantaneous tides and tidal currents, extremely efficient long-term simulations of transport phenomena using this model are feasible. Finally, the spectral model results compare well with published analytical solutions.

SELECTED REFERENCES

Blumberg, A.F., and Mellor, G.L., 1981, A numerical calculation of the circulation in the Gulf of Mexico: Princeton, N.J., Dynalysis of Princeton, Report 66, 153 p.

Cheng, R.T., 1978, Modeling of hydraulic systems by finite element methods: Advances in Hydro Science, v. 11, 207 p.

Cheng, R.T., and Casulli, Vincenzo, 1982, On Lagrangian residual currents with applications in South San Francisco Bay, California: Water Resources Research, v. 18, no. 6, p. 1652-1662.

Cheng, R.T., Feng, Shizuo, and Xi, Pangen, 1981, On Lagrangian residual ellipse *in* Kreeke, J. van de, ed., Lecture notes on coastal and estuarine studies: New York, Springer-Verlag, 280 p.

Cheng, R.T., and Gartner, J.W., 1985, Harmonic analysis of tides and tidal currents in South San Francisco Bay, California: Estuarine, Coastal and Shelf Science, v. 21, p. 57-74.

Chow, V.T., 1959, Open-channel hydraulics: New York, McGraw Hill, 680 p.
Cunge, J.A., Holly, F.M., and Verwey, Adri, 1980, Practical aspects of computational river hydraulics: Boston, Massachusetts, Pitman Advanced Publishing, 420 p.
Defant, Albert, 1919, Untersuchungen uber die Gezeiten Erscheinungen *in* Mittelund Randmeeren: in Buchten und Kanalen Teil I-IX, 96 p.
Dennis, R.E., and Long, E.E., 1971, A user's guide to a computer program for harmonic analysis of data at tidal frequencies: U.S. Department of Commerce, National Oceanic and Atmospheric Administration, National Ocean Survey, Technical Report NOS 41, Rockville, Maryland, 31 p.
Dronkers, J.J., 1964, Tidal computations in rivers and coastal waters: New York, John Wiley, 518 p.
Feng, Shizuo, Cheng, R.T., and Xi, Pangen, 1986, On tide-induced Lagrangian residual current and residual transport: Water Resources Research, v. 22, no. 12, p. 1623-1634.
Gray, W.G., and Lynch, D.R., 1977, Time stepping schemes for finite element tidal model computations: Advances in Water Resources, v. 1, 83 p.
-----1979, On the control of noise in finite element tidal computations: A semi-implicit approach: Computers and Fluids, v. 7, no. 1, p. 47-67.
Hansen, Walter, 1950, Tides, *in* Hill, M.N., ed.: The sea, physical oceanography, ideas and observations on progress in the study of the seas: New York, Interscience Publishers, chap. 23, p. 764-801.
Huebner, K.H., 1975, The finite element method for engineers: New York, John Wiley, 500 p.
Kawahara, Mutsuto, and Hasegawa, Kenichi, 1978, Periodic galerkin finite element method of tidal flow: International Journal for Numerical Methods in Fluids, v. 12, p. 115-127.
Kawahara, Mutsuto, Morihira, Michio, Kataoka, Shinji, and Hasegawa, Kenichi, 1981, Periodic finite elements in two-layer tidal flow: International Journal for Numerical Methods in Fluids, v. 1, p. 45-61.
King, I.P., Norton, W.R., and Orlob, G.T., 1973, A finite element solution for two-dimensional density stratified flow: Final report prepared for the U.S. Department of the Interior, Office of Water Resources Research, WRE 11360, v. 11360, 80 p.
La'Mehaute, Bernard, 1976, An introduction to hydrodynamics and water waves, New York, Springer-Verlag, 315 p.
Le Provost, Christian, and Poncet, Alain, 1978, Finite element method for spectral modeling of tides: International Journal for Numerical Methods in Fluids, v. 12, p. 853-871.
Leendertse, J.J., and Gritton, E.C., 1971, A water-quality simulation model for well-mixed estuaries and coastal seas, Volume 2, Computational procedures: New York, Rand Corp., 53 p.
Lynch, D.R., and Gray, W.G., 1979, A wave equation model for finite element tidal computations: Computers and Fluids, v. 7, no. 3, 207 p.
McCracken, D.D., and Dorn, S.D., 1964, Numerical methods and Fortran programming: New York, John Wiley, 457 p.

Pearson, C.E., and Winter, D.F., 1977, On the calculation of tidal currents in homogeneous estuaries: Journal of Physical Oceanography, v. 7, p. 520-531.

Pinder, G.F., and Gray, W.G., 1977, Finite element simulation in surface and subsurface hydrology: New York, Academic Press, 295 p.

Platzman, G.W., 1981, Some response characteristics of finite-element tidal models: Journal of Computational Physics, v. 40, p. 36-63.

Ponce, V.M., and Yabusaki, S.B., 1980, Mathematical modeling of circulation in two-dimensional plane flow, *in* Final Report to the National Science Foundation: Fort Collins, Colorado, Colorado State University, 289 p.

Pritchard, D.W., 1971, Hydrodynamic models, Sections 1 and 2, *in* Estuarine Modeling: An Assessment: Austin, Texas, TRACOR, Inc. (NTIS Report PB-206-807), p. 5-33.

Roache, P.J., 1982, Computational fluid dynamics: Albuquerque, New Mexico, Hermosa Publishers, 446 p.

Rodi, Wolfgang, 1984, Turbulence models and their application in hydraulics - A state of the art review: Karlsruhe, Federal Republic of Germany, University of Karlsruhe, 104 p.

Schlichting, Hermann, 1979, Boundary-layer theory: New York, McGraw-Hill, 817 p.

Schureman, Paul, 1985, Manual of harmonic analysis and prediction of tides reprinted with corrections, 1976: U.S. Coast and Geodetic Survey Special Publication 98, 317 p.

Sheng, Y.P., 1983, Mathematical modeling of three-dimensional coastal currents and sediment dispersion: Model development and application: U.S. Army Corps of Engineers Technical Report CERC-93-2, 288 p.

Smith, L.H., and Cheng, R.T., 1987, Tidal and tidally averaged circulation characteristics of Suisun Bay, California: Water Resources Research, v. 23, no. 1, p. 143-155.

Snyder, R.L., Sidjabet, M.M., and Filoux, J.H., 1979, A study of tides, set-up and bottom friction in a shallow semi-enclosed basin. Part II: Tidal model and comparisons with data: Journal of Physical Oceanography, v. 9, p. 170-188.

Tennekes, Hermann, and Lumley, J.L., 1972, A first course in turbulence: Cambridge, Massachusetts, The MIT Press, 300 p.

Walters, R.A., 1983, Numerically induced oscillations in finite element approximations to the shallow-water equations: International Journal of Numerical Methods in Fluids, v. 3, p. 591-604.

-----1986, A finite element model for tidal and residual circulation: Communications in Applied Numerical Methods: New York, John Wiley, p. 393-398.

Westerlink, J.J., Connor, J.J., and Stolzenbach, K.D., 1983, Harmonic finite element model of tidal circulation for small bays *in* Shen, H.T., ed., Proceedings of the Conference on Frontiers in Hydraulic Engineering: New York, American Society of Civil Engineers, p. 170-179.

White, F.M., 1979, Fluid mechanics: New York, McGraw-Hill, 701 p.

Zienkiewicz, O.C., 1979, The finite element method: New York, McGraw-Hill, 787 p.